The Impacts of Assimilating Fengyun-4A Atmospheric Motion Vectors on Typhoon Forecasts

Keyi Chen[1], Peigen Guan[1]

[1] School of Atmospheric Sciences, Chengdu University of Information Technology, Chengdu, China.

Corresponding author: Keyi Chen (ckydlt@aliyun.com)

Key Points:

- The data quality of AMVs from the FY-4A are assessed and compared with that from the FY-2G.
- Assimilating the AMVs from Fengyun satellites can slightly reduce the track errors.
- Assimilating the AMVs from Fengyun satellites has neutral to positive impacts extending from the upper to the lower level with time.

Abstract

Atmospheric motion vectors (AMVs), known as cloud track winds, have positive impacts on global numerical weather forecasts (NWP). In this study, AMVs retrieved from Fengyun-2G and Fengyun-4A are compared in their data quality and impacts on the typhoon forecasts in order to investigate the differences between the first and second generation of the geostationary meteorological satellites of China. This report conducted data evaluation and assimilation-forecasting experiments on FY-2G and FY-4A atmospheric motion vector (AMVs), respectively. The results show that the AMVs data of FY-4A are of better quality than those of FY-2G and assimilating the AMVs of FY-2G and FY-4A have a neutral to slightly positive impacts on typhoon forecasts, which is quite encouraging for the operational use in the future.

1 Introduction

As early as the 1970s, China began to research and develop meteorological satellites. By the end of 2021, China has successfully launched 19 meteorological satellites in total, 7 of which are in orbit, including three polar-orbiting satellites and four geostationary satellites operationally. Fengyun-4A (known as FY-4A) is the first one of China's second-generation geostationary meteorological satellites, which was successfully launched from Xichang Satellite Launch Base on December 11, 2016. On December 17, it was fixed in a geostationary orbit at 99.5°E over the equator. Since May 25, 2017, FY-4A drifted to the current position at 105°E for the operational use and its data and products were officially delivered to the users globally from September 25, 2017.

Compared with its predecessor (Fengyun-2 series) and other internationally geostationary satellites, Geostationary Interferometric Infrared Sounder (GIIRS) onboard FY-4A is the infrared hyperspectral sounder for the first time in geostationary orbit detecting atmospheric temperature, water vapor, gases, clouds, Earth surface radiations and so on. The advanced Geostationary Radiation Imager (AGRI) with 15 channels provides multi-purpose imagery and wind derivation by tracking clouds and water vapor features. FY-4A is also the first meteorological satellite in the world to achieve comprehensive observation of geostationary orbit imaging and infrared hyperspectral atmospheric vertical detection (Yang et al.,2012).

As a new member of Fengyun satellite series, FY-4A has attracted great research interests globally. Zhang et al. (2016) compared FY-4A with Japanese Himawari-8/9 satellites from four aspects of comprehensive detection, instrument observing ability, quantitative application and data service, and found that the two satellites had their own advantages and disadvantages, respectively. Through the study of AGRI/FY-4A, Lu et al. (2017) showed that the observing spectrum settings and spatio-temporal resolutions of the imagers are significantly improved comparing with the first generation of Fengyun satellites. Hansen M C et al. (2000) noticed that the newly added observation channel of AGRI provides a brand new observation support for monitoring atmospheric aerosol, dust/ash, cloud phase and fire point

Atmospheric motion vectors (AMVs) is one of the retrieved products of geostationary Fengyun satellite series. It is to retrieve the horizontal wind vectors of the different height levels by tracking the features on the successive multiple satellite images mainly from the infrared and water vapor channels (Xue, 2009). This retrieved product provides data supplement for the lack of wind measuring instruments, especially over the wide open ocean. Previously, meteorologists have studied the AMVs of Fengyun satellite series operationally and scientifically. Mecikalski et

al. (2006); Bedka et al. (2009); Mecikalski et al. (2010) evaluated meso-scale atmospheric motion wind vectors (MAMVs) and proposed that MAMVs could be used to study the convective mechanism. Height assignment was noted as the dominant factor for the main AMVs uncertainty suggested by Velden et al. (2009) when comparing the AMVs with the conventional wind profiles. Aiming to provide detailed uncertainty estimates for the assigned pressure, Salonen et al. (2015) proposed that best-fit pressure statistics enable reliable information about the AMV uncertainties in the height assignment, which was an effective method independent on different data assimilation systems convinced by the Met Office and European Centre for Medium-Range Weather Forecasts (ECMWF) systems. Liu et al. (2012) used Weather Research and Forecasting Model Data Assimilation (WRFDA) system to assimilate the AMVs data retrieved from FY-2C infrared and water vapor channels, and showed that the reasonable selection of AMVs data added to the numerical weather prediction (NWP) model was beneficial to supply the meso-scale information not included in the initial fields, as well as improving the prediction ability of the model. In order to assess the qualities and assimilating impacts of the AMVs retrieved from the first generation of the Chinese Fengyun geostationary satellite, the AMVs data of FY-2G and Himawari-8 were evaluated by Liang et al. (2021) in typhoon forecasts with the conclusions that both AMVs data have showed comparably positive forecasting impacts even though the AMVs quality of Himawari-8 were overall better.

As a type of indirect satellite observation data products, the AMVs can be applied in the assimilation system in order to provide the important wind information at different height levels, but few study used the AMVs of FY-4A in the NWP. Therefore, this paper will focus the assimilating and forecasting impacts of the AMVs of FY-4A. The AMVs data set of Fengyun satellite series and the NWP model for research and methodology used in this study are described in the following section. Basic pre-processes before AMVs data assimilation and data sets assessment will be conducted in the section 3. In Section 4, we selected typhoon In-Fa to study the assimilation and forecasting impacts of assimilating the AMVs data of FY-2G and FY-4A on typhoon prediction. Those impacts are verified in typhoon Haishen case in section 5 and this study concludes in second 6.

2 Data and Methodology

2.1 WRFDA-3DVAR Assimilation System

The Weather Research and Forecasting Model (WRF) model and Weather Research and Forecasting Model Data Assimilation (WRFDA) system (Barker et al., 2012) (Version 3.9.1) are applied for this study by using the 3DVAR component, which can assimilate most of the conventional observation data and part of the non-conventional observation data (Barker et al., 2003; Huang, X.Y. et al., 2009; Barker et al., 2012). To obtain a statistically optimal analysis, an iterative minimization of a prescribed cost function is described by:

$$J(x) = 1/2[(x-x^b)^T B^{-1}(x-x^b)+(y-H[x])^T R^{-1}(y-H[x])] \quad (1)$$

where x represents the atmospheric state vector, xb represents the background state, H represents the nonlinear observation operator which maps the model variables to the observation space, and y represents the observation vector. B and R represent the background and observation error covariance matrices, respectively.

97 2.2 AMVs Data Sets from Fengyun Satellite Series

98 The AMVs data of FY-2G and FY-4A both retrieved from infrared and water vapor
99 channels provided by The National Satellite Meteorological Center of China (NSMC) are studied
100 in this report with the aim to compare the assimilating impacts from the first and second
101 generation of geostationary satellites on typhoon prediction. The AMVs data of FY-2G are
102 retrieved from images of one infrared channel (10.3-11.3μm) and one water vapor channel (6.3-
103 7.6μm) with a time resolution of 6h(0000 UTC, 0600 UTC, 1200 UTC, 1800UTC) and a
104 horizontal resolution of 110KM; while the AMVs of FY-4A are retrieved from images of one
105 infrared channel (10.3-11.3μm) and two vapor channels (6.9-7.3μm, 5.8-6.7μm) with a higher
106 time resolution of 3h(0000 UTC, 0300 UTC, 0600 UTC, 0900 UTC, 1200 UTC, 1500 UTC,
107 1800 UTC, 2100 UTC) and the horizontal resolution of 64 km. All retrieved AMVs are divided
108 into three layers: 100-400 hPa for high-level, 400-700 hPa for middle level, and 700-950 hPa for
109 lower level and each AMVs data contains latitude, longitude, height, U component, V
110 component, wind speed, wind direction and quality mark QI with a value range from 0 to 100.
111 Basically, the larger QI value is, the smaller error of the wind vector will be and the AMVs with
112 QI larger than 80 are considered to be of good quality. The parameters of the two satellites are
113 listed in Table 1 and the observing regions of the two satellites are shown in Figure 1. The red
114 circle and the yellow one indicate the observation area of FY-2G and FY-4A, respectively, and
115 the green rectangle domain is the overlapped observing area of the two satellites, as well as the
116 studied regions in this report.

117 Table 1: The channels used for retrieving the AMVs of geostationary satellite FY-2G and
118 FY-4A.

Satellite	IR Channel (μm)	WV Channel (μm)	Observing Area	Nadir
FY-2G	10.3-11.3	6.3-7.6	55°E-155°E 50°S-50°N	99.5°E
FY-4A	10.3-11.3	6.9-7.3 5.8-6.7	40°E-170°E 65°S-65°N	105°E

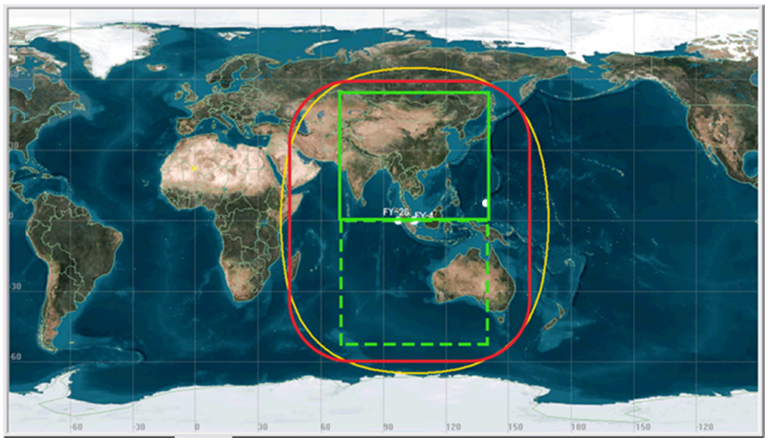

Figure 1. The observation area of geostationary satellites FY-2G and FY-4A (the red circle is for FY-2G; the yellow circle is for FY-4A; the green box is the studied area here; the solid line is for the northern hemisphere; the dotted line is for the southern hemisphere).

2.3 Reanalysis Data

The final (FNL) operational global analysis data provided by the National Center for Environmental Prediction (NCEP) are used to initialize the WRF model and update the lateral boundaries in this study and have a temporal resolution of 6h (0000 UTC, 0600 UTC, 1200 UTC, 1800UTC), a spatial resolution of 0.25°x 0.25° and 26 vertical levels from 1000hPa to 10hPa. This product is from the Global Data Assimilation System (GDAS), which continuously collects observational data from the Global Telecommunications System (GTS), and other sources (see more details at https://rda.ucar.edu/datasets/ds083.2/). Parameters in the analyses includes surface pressure, sea level pressure, geopotential height, temperature, sea surface temperature, soil values, ice cover, relative humidity, u- and v- winds, vertical motion, vorticity and ozone, except any AMVs information of Fengyun geostationary satellite series (https://www.emc.ncep.noaa.gov/gmb/STATS/html/model_changes.html).

The ERA-5 (1950-present) global reanalysis data from the European Centre for Medium-Range Weather Forecasts (ECMWF) are used as an independent reference data for verifying the AMVs data quality of the two Fengyun geostationary satellites. The selected time resolution for this study is 6h (0000 UTC, 0600 UTC, 1200 UTC, 1800UTC), spatial resolution is 0.25°x 0.25°, and vertical levels are from 1000 hPa to 1 hPa as mentioned above (https://confluence.ecmwf.int/pages/viewpage.action?pageId=74764925).

2.4 Typhoon Track and Intensity Data

The best track data of typhoons provided by the China Meteorological Administration Tropical Cyclone Database ("CMA best track" is used thereafter for simplicity) with 6-hour intervals are used to evaluate the prediction results of the track and intensity of the typhoons.

3 The Assessment of the AMVs Data

Similar to the previous studies (Liang et al., 2021), the AMVs data retrieved from both Fengyun geostationary satellites have the largest number at the upper level (100-400hPa), as well as the AMVs with QI>80 from both satellites, regardless of the retrieving channels (the figures are not shown). The wind speed bias and root mean square error (RMSE) distribution of the

AMVs data from the two satellites (using the AMVs retrieved from the infrared channels as an example) in the studied green rectangle area of Figure 1 are displayed in Figure 2, referring to the ERA-5 global reanalysis data. In order to avoid the seasonal differences of the Northern and Southern Hemisphere, the wind speed bias and RMSE of the two satellites are compared within the same hemisphere, respectively.

Apparently, FY-2G AMVs data with QI > 80 have dominantly better quality by showing smaller and more stable RMSE vertically than those with smaller QI (Figure 2a), while FY-4A AMVs data with different QI are generally comparable from the lower levels to the upper ones (Figure 2b). Though the RMSE of FY-4A AMVs data with lower QI values are slightly smaller than those with QI > 80 above 200hPa and below 475hPa, the biases of the former is much smaller than the latter regarding to the whole atmospheric levels (Figure 2d). Comparatively, the biases of FY-2G AMVs data with QI > 80 are larger with the value range from -7m/s to 4m/s. Similar results are found for the AMVs data retrieved from the water vapor channels of the two geostationary satellites and for the studied southern Hemisphere area. This indicates that the overall quality of the AMVs data from FY-4A as the second generation meteorological satellite of China is improved than those from the first generation satellite FY-2G.

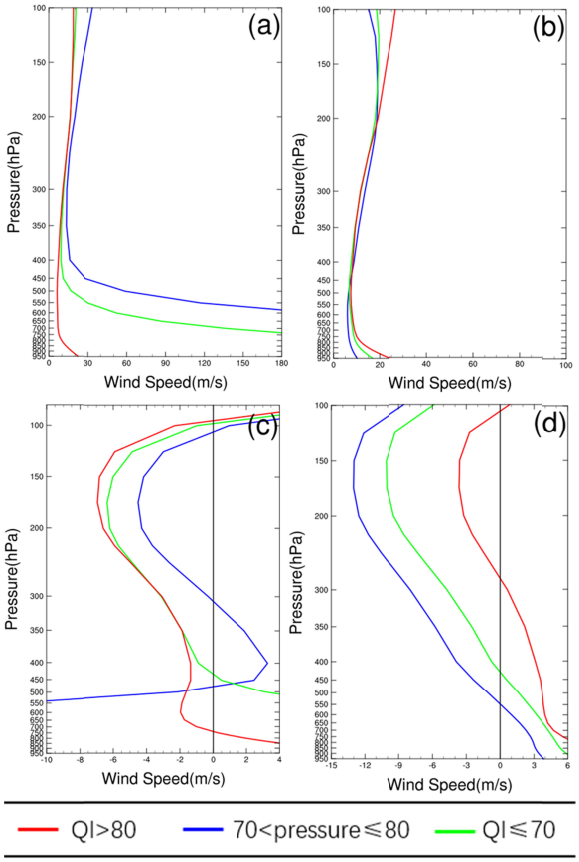

Figure 2. The vertical distributions of the RMSE (upper row) and the bias (lower row) of the full wind speed of the AMVs data retrieved from the infrared channels for the Northern Hemisphere referring to the ERA5 global reanalysis data. ((a) and (c) are for FY-2G, and (b) and (d) are for FY-4A. Red line represents the AMVs with QI larger than 80, blue line represents the AMVs with QI between 70 and 80, green line represents the AMVs with QI smaller than 70.

The RMSE time series of the AMVs data retrieved from the infrared channels of the two satellites at different height levels from August 1 2020 to October 31 2020 are described in Figure 3. Similarly to the previous results, the RMSE and its variations with time of the AMVs data from FY-4A at different levels are quite comparable regardless of their QI values. Compared to those from FY-2G, the RMSE values of FY-4A AMVs data are much smaller with a smaller time variation. For FY-2G AMVs data, only those with QI > 80 show reliable data quality. This further demonstrates that the AMVs data of FY-4A have better and more reliable quality than those of the first generation of Fengyun geostationary satellites..

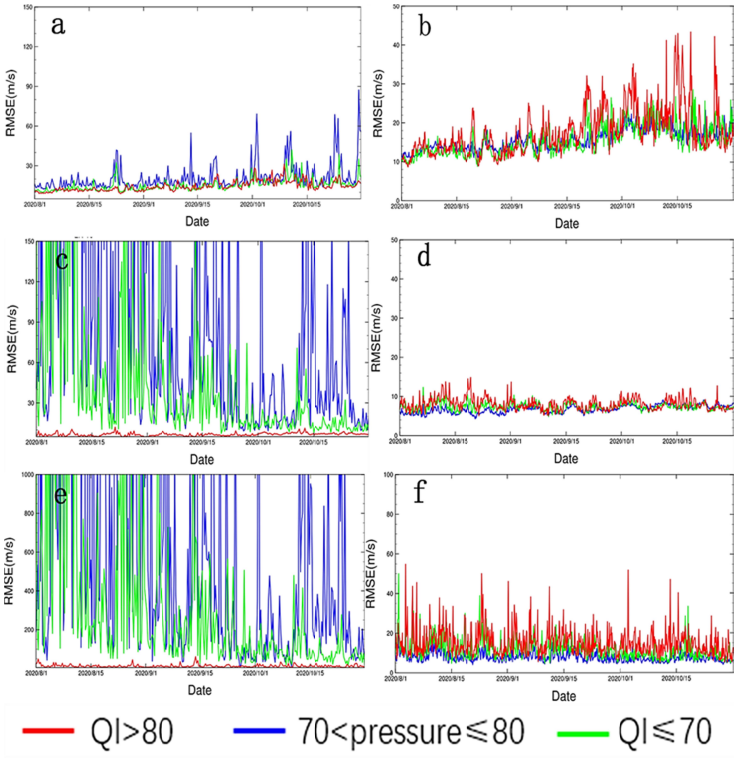

Figure 3. The RMSE time series of the AMVs data retrieved from the infrared channels at different height levels from August 1 2020 to October 31 2020. The red line represents the AMVs data with QI larger than 80; the blue line represents the AMVs data with QI between 70 and 80; and the green line represents the AMVs data with QI smaller than 70. (a), (c), (e) are for FY-2G and (b), (d), (f) are for FY-4A. The upper row are for 100 ~400hPa; the middle row are for 400 ~700hPa; and the lower row are for 700 ~950hPa.

Considering the AMVs data characteristics, a series of quality control processes, including height assignment, quality control, background check, observation error assignment, channel merging and thinning, are conducted referring to Liang et al.(2021).

The WRFDA-3DVAR assimilation system applied in this paper requires that the assimilated AMVs data are unbiased (Gaussian distribution). Figure 4 shows the Probability density distribution (PDF) of the first guess departures (O-B) of the AMVs data retrieved from the infrared channels of FY-2G and FY-4A after quality control processes at 12:00 UTC on July 22 2020 (similar results for water vapor channels, not shown). Undoubtedly, the PDF of FY-4A is more unbiased with a much narrower normal shape than that of FY-2G and also the first guess

departures of the combined AMVs data of the two satellites meet the unbiased requirements of the 3DVAR method, which insures that the assimilating experiments can be carried out.

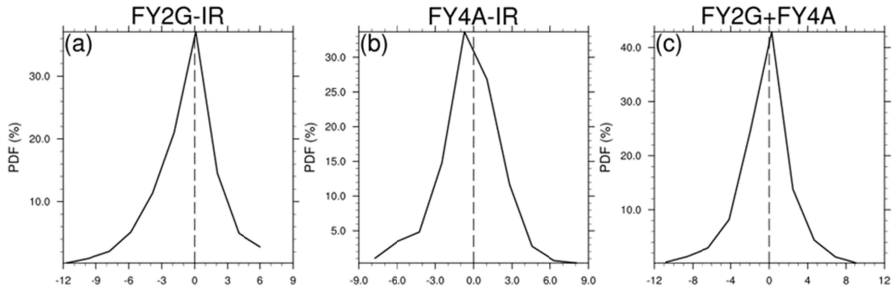

Figure 4. The Probability density distribution of the first guess departures (O-B) of the AMVs data retrieved from the infrared channels of FY-2G and FY-4A after quality control processes at 12:00 UTC on July 22, 2020 (a for FY2G, b for FY4A, and c for the combined FY2G and FY4A).

4 AMVs Data Assimilation Experiments Studies

4.1 Overview of Severe Typhoon In-Fa

Typhoon In-Fa, the 6th typhoon forming in the Western Pacific Ocean in 2021 had a predominantly northwestward path (Figure 5), which is selected to study the assimilating and forecasting impacts of AMVs from the two Fengyun geostationary satellites. At 0200 UTC on July 18, the Central Meteorological Agency (CMA) upgraded it to a tropical storm based on the observations and then upgraded it to a strong typhoon at 1100 UTC on July 21. Typhoon In-Fa made its landfall on the coastal of Zhejiang Province at 1200 UTC on July 25, and made landfall again on the coastal area of Pinghu county, Zhejiang Province at 0900 UTC on July 26. In-Fa weakened in Anhui province on July 28 and then gradually moved northwestward. The main characteristics of Typhoon “In-Fa” include slow moving speed, long retention time over land, and large cumulative rainfall. A total of 4.82 million people in Zhejiang, Shanghai and Jiangsu provinces were affected by Typhoon In-Fa, with a direct economic loss of 13.2 billion RMB.

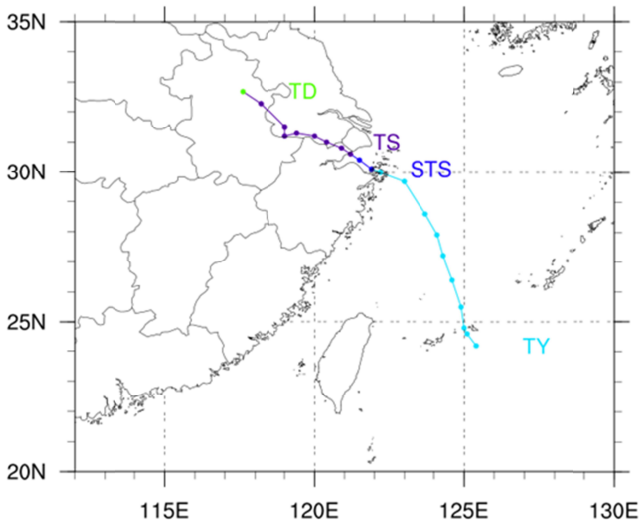

Figure 5. The CMA best track of In-Fa from 0000 UTC on July 23, 2021 to 2100 UTC on July 27, 2021 (interval: 6h; TD: Tropical Depression TS: Tropical Storm; STS: Severe Tropical Storm; TY: Typhoon).

4.2 Experimental settings

To compare the assimilating and forecasting impacts of the retrieved AMVs data from different channels of the two Fengyun geostationary satellites on the forecasts of Severe Typhoon In-Fa, 9 experiments are set up, including one control experiment and 8 cycling assimilation experiments with assimilating the AMVs data retrieved from infrared and water vapor imaging channels of FY-2G and FY-4A, respectively (Table 2). FY2G-IR, FY2G-IR+WV and FY2G+FY4A are used to illustrate the assimilating experiment settings. FY2G-IR indicates that the AMVs data retrieved from the infrared images of FY-2G satellite are assimilated in the cycling experiment, while the AMVs data retrieved from the infrared and water vapor images of FY-2G are assimilated in FY2G-IR+WV experiment and all the AMVs data from both FY-2G and FY-4A satellites are assimilated in FY2G+FY4A experiment regardless the retrieved channels.

Table 2: The List of the Assimilating Experiment Settings.

Experiments	ID	Settings
Control experiment	CONT	Without data assimilated
cycling assimilation experiments	FY2G-IR	FY-2G AMVs data from the infrared channel assimilated
	FY2G-WV	FY-2G AMVs data from the water vapor channel assimilated
	FY2G-IR+WV	FY-2G AMVs data from the combined channels assimilated
	FY4A-IR	FY-4A AMVs data from the infrared channel assimilated
	FY4A-WV1	FY-4A AMVs data from the lower water vapor channel assimilated
	FY4A-WV2	FY-4A AMVs data from the higher water vapor channel assimilated

	FY4A-IR+WV	FY-4A AMVs data from the combined channels assimilated
	FY2G+FY4A	FY-2G+FY-4A AMVs data from all the five retrieved channels assimilated

The model integration time is from 0000 UTC on July 22 2021, after the tropical storm was strengthened to Typhoon In-Fa, to 0000 UTC on July 28 2021, after its landfall and weakening, for the all nine experiments, with the model configuration including 300×300 grids centering at (28°N, 120°E), the horizontal resolution of 15km, the time step 60 seconds, the 40 eta layers in the vertical direction and the model top at 10hPa.

The cycling analysis-forecast experiments starting from 1200 UTC on July 22 2021 with the AMVs data assimilated every 12h are carried out with different settings. Except the first 12 hours for the spin-up time, nine DA cycles are performed in total with a 6h assimilating window. The National Meteorological Center method (NMC; Parrish & Derber,1992) is applied to assign the background error covariance by calculating the forecast differences between the 24-h and 12-h forecasts. The background for the first analysis is the forecast initiated from the FNL analysis at 1200UTC on July 22 2021 and the backgrounds for the following cycles are the 12h model forecasts initialized from the previous analyses of last cycles. In addition, table 3 lists the physical parameterization schemes adopted in all nine assimilating experiments.

Table 3: The List of the Parameterization Schemes Used for All the Nine Experiments for Typhoon In-Fa.

parameterization schemes	settings
Microphysics scheme	Lin (Lin et al, 1983)
Cumulus convection scheme	Tiedtke (Tiedtke, M. et al., 1989)
radiation scheme	RRTMG /RRTMG (Mlawer et al., 1997)
Planetary boundary layer scheme	MYJ (Janjic et al., 1994)
Land-surface scheme	Noah (Niu et al., 2011)

4.3 Forecasting Impacts on Typhoon In-Fa

4.3.1 Impacts on the Typhoon Track and Intensity Forecasts

Figure 6 displays the forecasting tracks of Typhoon In-Fa in all nine experiments verified by the CMA best track data since In-Fa made its landfall in East China. Basically, the results of the eight cycling assimilation experiments are slightly better compared to the control run by showing tracks closer to the CMA data (Figure 6a and 6b). Before the landfall, those eight

forecasting tracks in the assimilation runs are quite comparable and track differences are more clear after the landfall which might be due to the impacts of the surfaces. Undoubtedly, the forecasting typhoon paths in FY2G-IR+WV and FY4A-IR+WV perform the best in their group and experiment FY2G+FY4A shows the best typhoon track overall with the most AMVs assimilated for the best fitting in this study. Compare 6a and 6b, the forecasted typhoon moving speeds in FY4A assimilating experiments (Figure 6b) are slower than those in FY2G assimilating experiments (Figure 6a) after the typhoon makes landfall. From the perspective of typhoon track forecasts, assimilating the AMVs of FY-2G and FY-4A can significantly improve the deviation of typhoon track simulation than the control experiment, effectively improve the typhoon path and make the forecast path closer to the real situation of the typhoon movement, but the slower moving speeds in the assimilating experiments which contain FY4A AMVs need to be further investigated to know the reason.

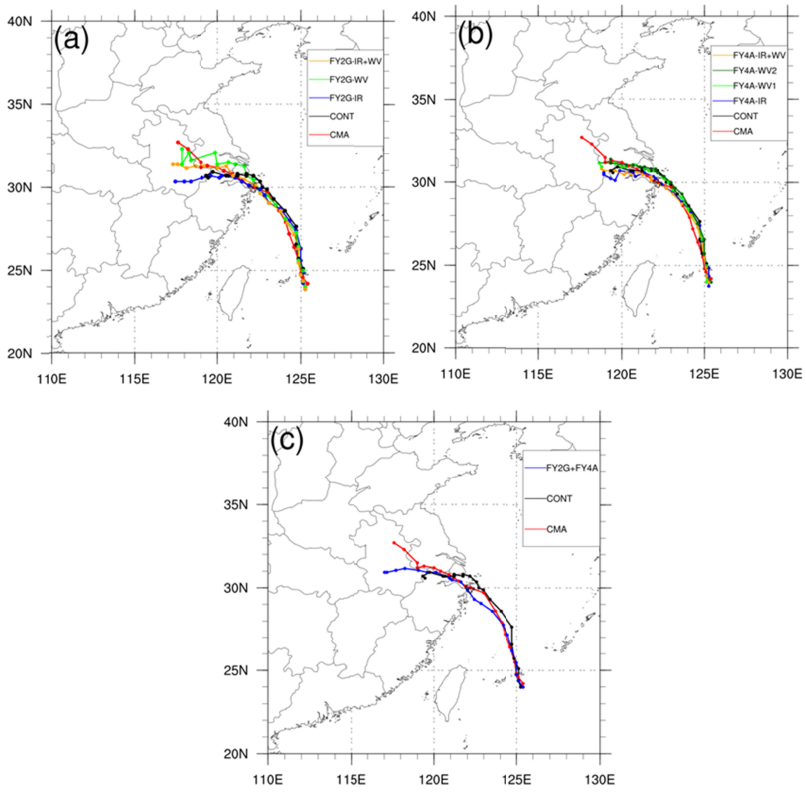

Figure 6. The evolution of track (a-c) referring to the CMA best track of Typhoon In-Fa from 0000 UTC on July 23 2021 to 0000 UTC on July 28 2021 (interval:6h; red: CMA best track; black: CONT; for a-c). For (a), yellow line represents experiment FY2G-IR+WV; green line represents experiment FY2G-WV; blue line represents experiment FY2G-IR. For (b), yellow line represents experiment FY4A-IR+WV; light blue line represents experiment FY4A-WV2; green line represents experiment FY4A-WV1; blue line represents experiment FY4A-IR. For (c), blue line represents experiment FY2G+FY4A.

At present, forecasts of typhoon intensity are still a difficult problem for each operational center. As shown in Figure 7a, the control and the assimilation experiments have similar intensity variation trends of typhoon In-Fa by overestimating the typhoon intensity at the early stage and approaching to the best track provided by the China Meteorological Agency (CMA)

since 1800 UTC on July 24 2021. From the perspective of typhoon intensity forecasts, assimilating the AMVs of FY-2G and FY-4A have neutral impacts.

In order to accurately compare the differences of typhoon track forecasts between all experiments, Figure 7b and 7c shows the track error (unit: km) of each experiment. Assimilating the AMVs from the merged channels (i.e. FY2G-IR+WV, FY4A-IR+WV, FY2G+FY4A) does indicate some benefits by showing generally smaller track errors, which also grow more slowly, than CONT, especially from 1800 UTC on July 25. Interestingly, 1800 UTC on July 25 is like a pitch point, before which the variations of the track errors in the eight cycled assimilating experiments are quite comparable regardless of the satellites and channels. While afterwards, the experiments with FY2G AMVs data assimilated achieve better results than those with FY4A AMVs, which may be as a results of that the forecasting typhoon moving speeds in FY4A assimilating experiments are slower than those in FY2G runs after the simulated landfall of typhoon.

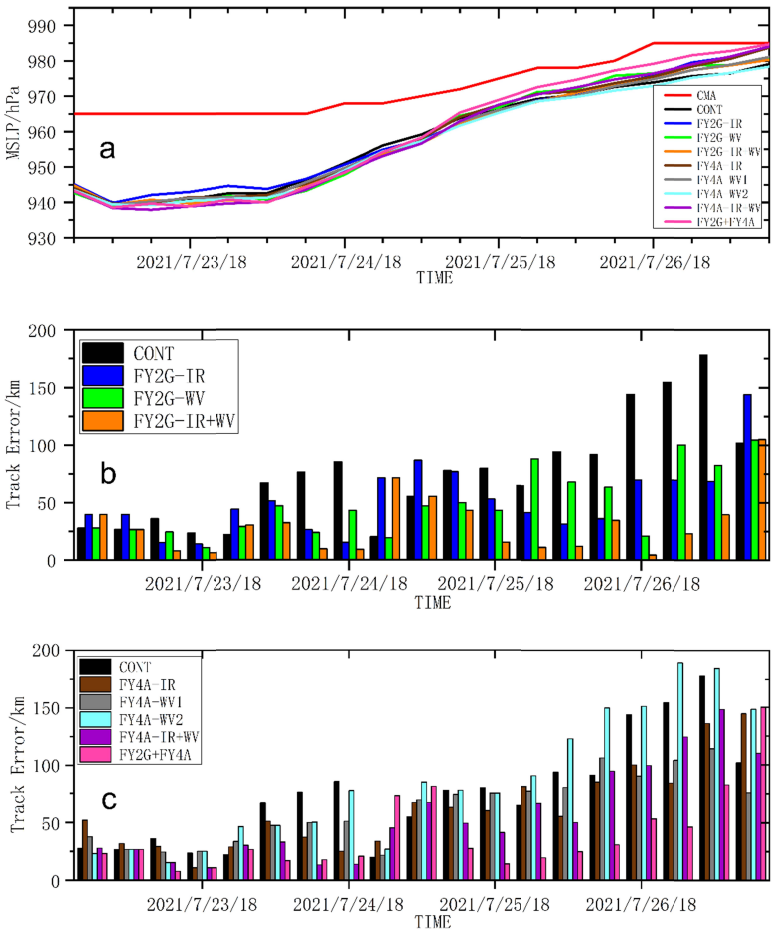

Figure 7. The evolution of intensity (MSLP, unit: hPa) and track errors (b-c unit: km) referring to the CMA best track data of Typhoon In-Fa from 0000 UTC on July 23 2021 to 0000 UTC on July 28 2021, the time interval is 6h. (black line and bar: CONT; blue line and bar: FY2G-IR; green line and bar: FY2G-WV; orange line and bar: FY2G-IR+WV; brown line and bar: FY4A-IR; grey line and bar: FY4A-WV1; light blue line and bar: FY4A-WV2; purple line

and bar: FY4A-IR+WV; pink line and bar: FY2G+FY4A; for a-c). For (a), red line represents the CMA best track.

4.3.2 Impacts on the Typhoon Precipitation Forecasts

As indicated by the observations of the hourly intensive automatic rainfall stations of the CMA (China Meteorological Administration) (Figure 8a), heavy precipitation over 100 mm mainly occurred in the east coast of China with the precipitation region located in Jiangsu and Anhui provinces. However, the precipitation in CONT is much underestimated than the observations (Figure 8b). While, all assimilating experiments overestimate the rainfall amount, which might be related to the overestimation of the typhoon intensity in each run, except that the experiment FY2G+FY4A corrects this kind of precipitation overestimation to some extent with the closest typhoon intensity to the CMA data. Comparing among the results with assimilating the AMVs from different channels, the experiments with those from water vapor channels (Figure 8d 8g 8h) are more likely to cause excessive precipitation forecasts than those from infrared channels (Figure 8c and 8f), which may be due to that the AMVs of the water vapor channel lack of the wind field information in the middle and lower levels of the atmosphere.

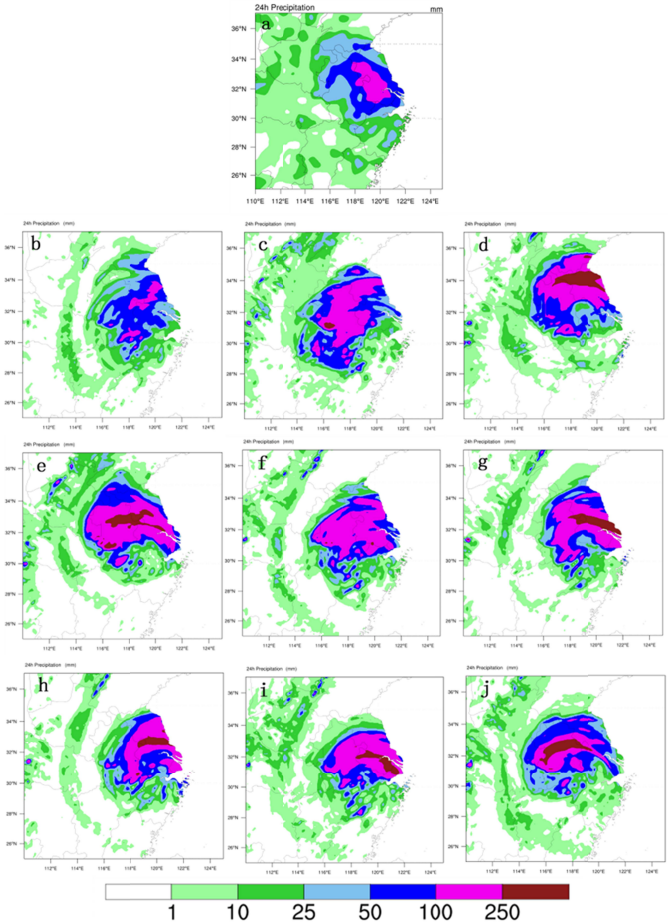

Figure 8. The 24-h accumulated precipitation (unit: mm) over land from 0000 UTC on July 27, 2021 to 0000 UTC on July 28, 2021 from CMA observations of the hourly intensive automatic rainfall stations (a), CONT (b), FY2G−IR (c), FY2G-WV (d), FY2G-(IR+WV) (e), FY4A−IR (f),FY4A-WV1 (g),FY4A-WV2(h),FY4A-(IR+WV)(i) and FY2G+FY4A(j) experiments.

4.3.3 Forecasting Impacts on the Physical Variables Fields

The vertical profiles of the root mean square error (RMSE) at 24-h, 72-h and 120-h forecasts of temperature, geopotential height, relative humidity and full wind speed started from 0000 UTC on July 23 2021 referring to the ECMWF ERA5 reanalysis data in the control run and eight assimilating experiments are calculated in order to quantitatively evaluate the assimilating and forecasting impacts on the longer-period forecasts and the values smaller than those of CONT indicate the positive impacts (Figure 9). Basically, the impacts on geopotential height and temperature are neutral from the lower level to the upper level with the time evolution. For the relative humidity field, slightly positive impacts are shown at 72-h forecast above 350hPa, which propagate down to near surfaces, and more evident improvements are displayed at 120-h forecasts for the entire vertical atmospheric levels. More dominantly positive impacts on the full wind speed occur above 450hPa at 24-h forecast, and extend to all levels at 72-h forecast, then become much more dramatic at 120-h forecast. Apparently, assimilating the AMVs data from the two Fengyun geostationary satellites in all experiments improves the most of the full wind speed forecasts than the forecasts of other physical variable fields vertically and the impacts extend from the upper level down to the lower level with the forecasting time evolution, for that there are the largest AMVs data amounts at the upper level. FY2G+FY4A experiment shows generally better positive impacts over all than others, which may be in the result of that the most observations assimilated provide a better fitting for the analysis.

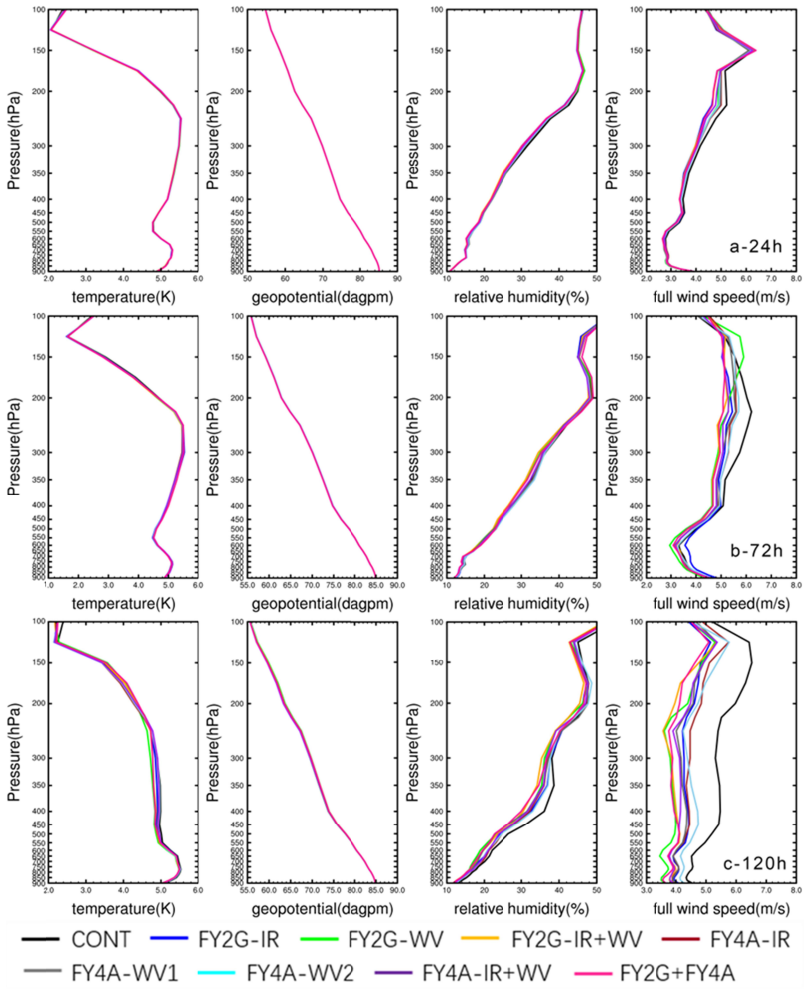

Figure 9. Vertical profiles of the 24-h (a), 72-h (b), and 120-h (c) forecast RMSEs referring to the ECMWF ERA5 reanalysis data of temperature (unit: K), geopotential height (unit: dagpm), relative humidity (unit: %) and the full wind speed (unit: m s−1) fields started from 0000 UTC on July 23 2021 from the control experiment (CONT) (black), FY2G − IR (blue),FY2G − WV (green), FY2G − IR + WV (yellow), FY4A − IR (dark purple), FY4A− WV1 (gray), FY4A-WV2(light blue), FY4A_IR+WV(purple) and FY2G+FY4A(purple red).

5 Verification of the Assimilation Impacts on Typhoon Forecasts

The results above demonstrate that the main impacts of assimilating the AMVs data from the two Fengyun geostationary satellites are neutral to slightly positive and basically the more AMVs data assimilated, the more improvements are shown. Aiming to verify this, more assimilating experiments are conducted. A series experiments for typhoon Haishen which is the 10th typhoon occuring in the Western Pacific Ocean in 2020 are studied here as a verification case. Haishen had a predominantly northward path (Figure 10). 9 experiments are also set up (Table 2) as mentioned above and the physical parameterization schemes adopted in all nine experiments are listed in Table 4.

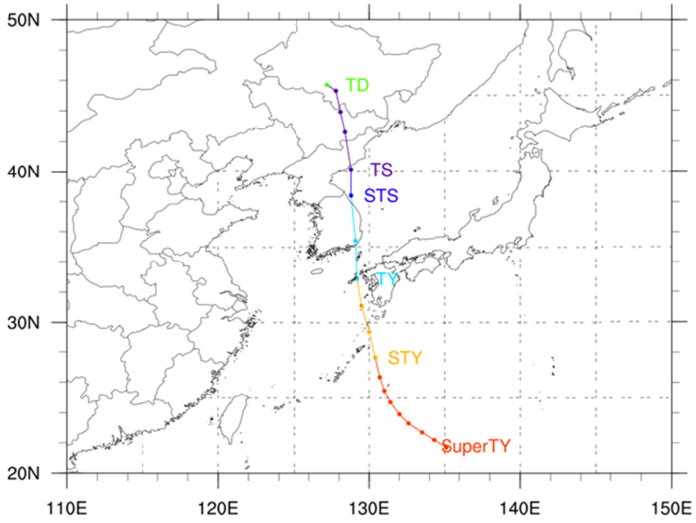

Figure 10. The CMA best track of Haishen from 0000 UTC on September 4, 2020 to 1200 UTC on September 8, 2020 (interval: 6h; TD: Tropical Depression; TS: Tropical Storm; STS: Severe Tropical Storm; TY: Typhoon STY: Severe Typhoon; SuperTY: Super Typhoon).

Table 4: The List of the Parameterization Schemes Used for all the Nine Experiments for Typhoon Haishen.

The Physical Parameterization Schemes		Configurations
Microphysics Scheme		Lin (Lin et al., 1983)
Planetary Boundary Layer Scheme		Yonsei University scheme (Hong et al., 2006)
Radiation Scheme	Long-wave	RRTM scheme (Mlawer et al., 1997)
	Short-wave	Dudhia scheme (Dudhia, 1989)

Cumulus Convection Scheme	Kain-Fritsch scheme (Kain, 2004)
Land-Surface Scheme	MM5 similarity (Fairall et.al., 2003)

Compared to the best track, the typhoon tracks in CONT and all assimilating experiments are almost the same with the best track for the first 48h (before 1200 UTC on September 5, 2020) before they start to deviate (Figure 11). While, the typhoon track forecasts of all assimilation experiments start to approach to the best track than that in CONT since 0000 UTC September 7 2020, especially for the experiments FY4A-IR+WV and FY2G+FY4A. Basically, more neutral to slightly positive impacts of forecasting and assimilation are still displayed with time varying, even with such a number of the AMVs data assimilated in each experiment.

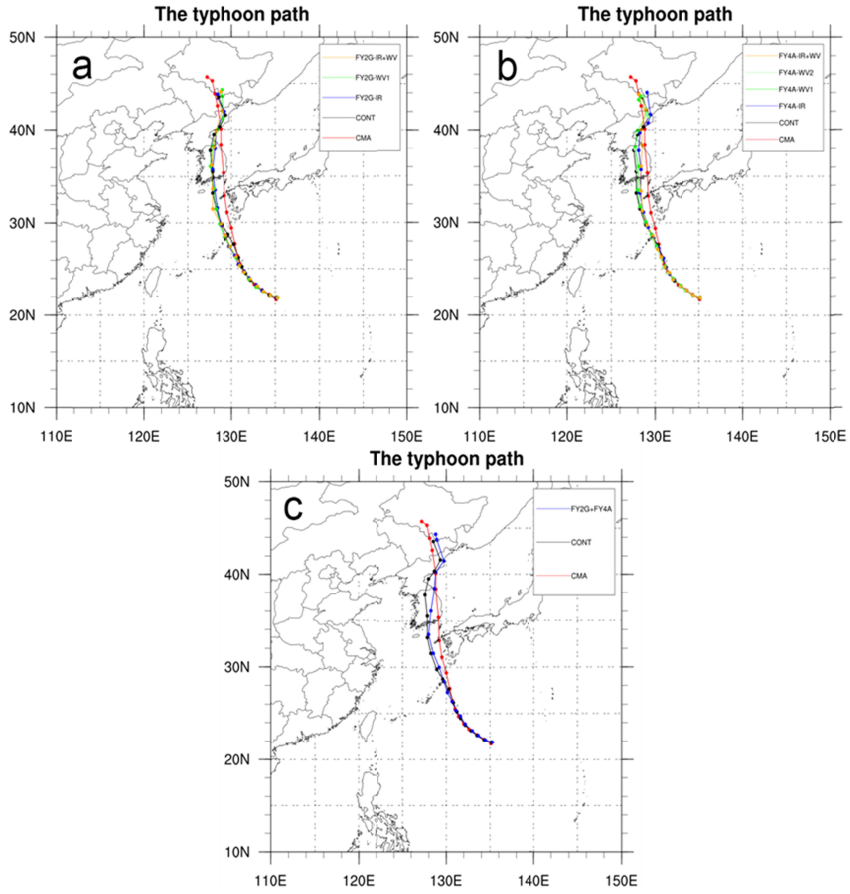

Figure 11. The evolution of track (a-c) referring to the CMA best track of Typhoon Haishen from 0000 UTC on September 4, 2020 to 1200 UTC on September 8, 2020 (interval:6h; red: CMA best track; black: CONT; for a-c). For (a), yellow line represents experiment FY2G-IR+WV; green line represents experiment FY2G-WV; blue line represents experiment FY2G-IR. For (b), yellow line represents experiment FY4A-IR+WV; light blue line represents experiment FY4A-WV2; green line represents experiment FY4A-WV1; blue line represents experiment FY4A-IR. For (c), blue line represents experiment FY2G+FY4A.

As shown in Figure 12a, compared with the intensity evolution of Typhoon Haishen provided by the CMA Tropical Cyclone Data Center., the control and assimilation experiments have similar intensity variation trends, but the occurrence time of the lowest MSLP is later in all

assimilation experiments than that in the best track data. Generally, the results of all cycling experiments are comparable, but slightly better forecasts are shown by the experiments with assimilating FY-4A AMVs data, and the best track forecasts are obtained from Experiment FY4A-IR+WV (Figure 12c), which indicates the advantages of channel merging. It also verifies that FY-4A, as China's second-generation meteorological satellite, has improved the data quality compared with FY-2G.

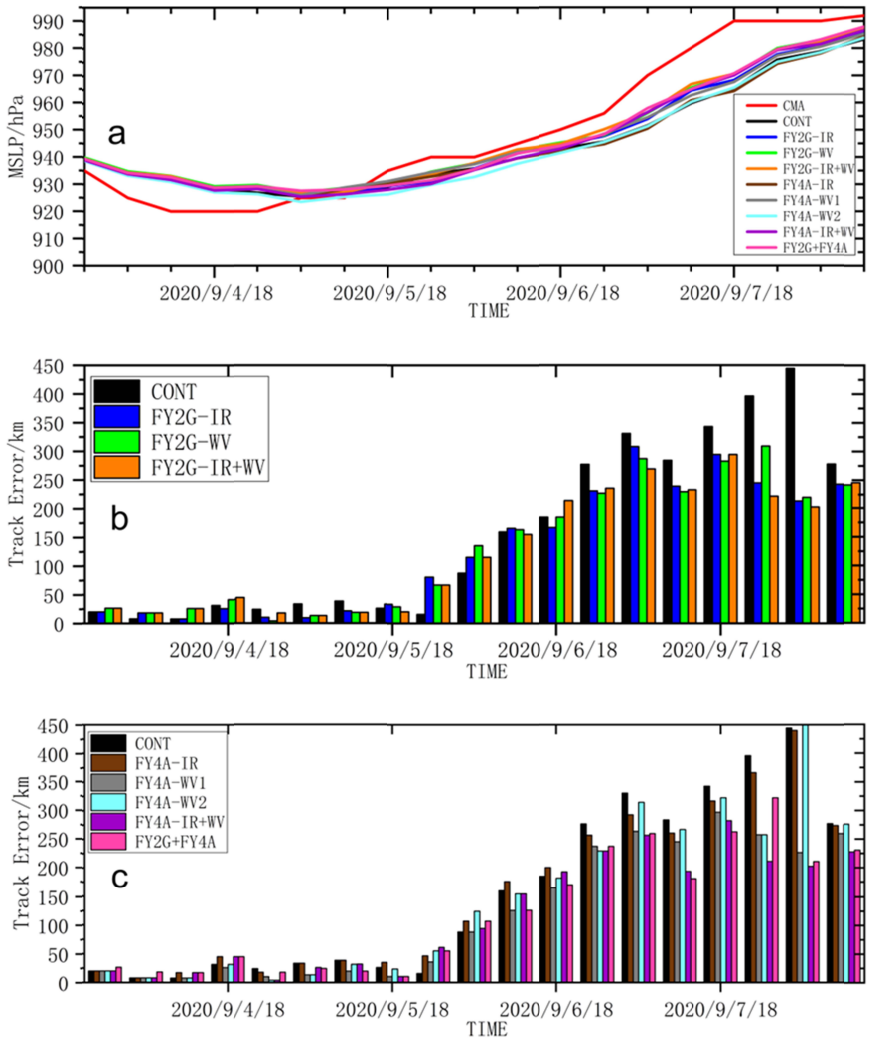

Figure 12. The evolution of intensity (a MSLP, unit: hPa) and track errors (b-c unit: km) referring to the CMA best track of Typhoon Haishen from 0000 UTC on September 4, 2020 to 1200 UTC on September 8, 2020 (black: CONT; blue: FY2G-IR; green: FY2G-WV; orange: FY2G-IR+WV; brown: FY4A-IR; grey: FY4A-WV1; light blue: FY4A-WV2; purple: FY4A-IR+WV; pink: FY2G+FY4A; for a-c). For (a), red line represents CMA best track.

For the forecast impacts on the physical variable fields, comparable improvements are still achieved in all assimilation experiments for the full wind speed. Slightly positive impacts on the full wind speed occur above 300hPa at 24-h forecast, and extend to 600hPa at 120-h forecast. The longer the forecast time is, the more positive impacts are shown (Figure 13). Similar to the previous results, assimilating the AMVs data from the two Fengyun geostationary satellites has

neutral to slightly positive impacts vertically on the full wind speed more evidently than other physical variables fields and the impacts extend from the upper level down to the lower level, since there are the largest AMVs data at the upper level. Though the main impacts are generally neutral, FY2G+FY4A experiment still shows a bit better positive impacts than others.

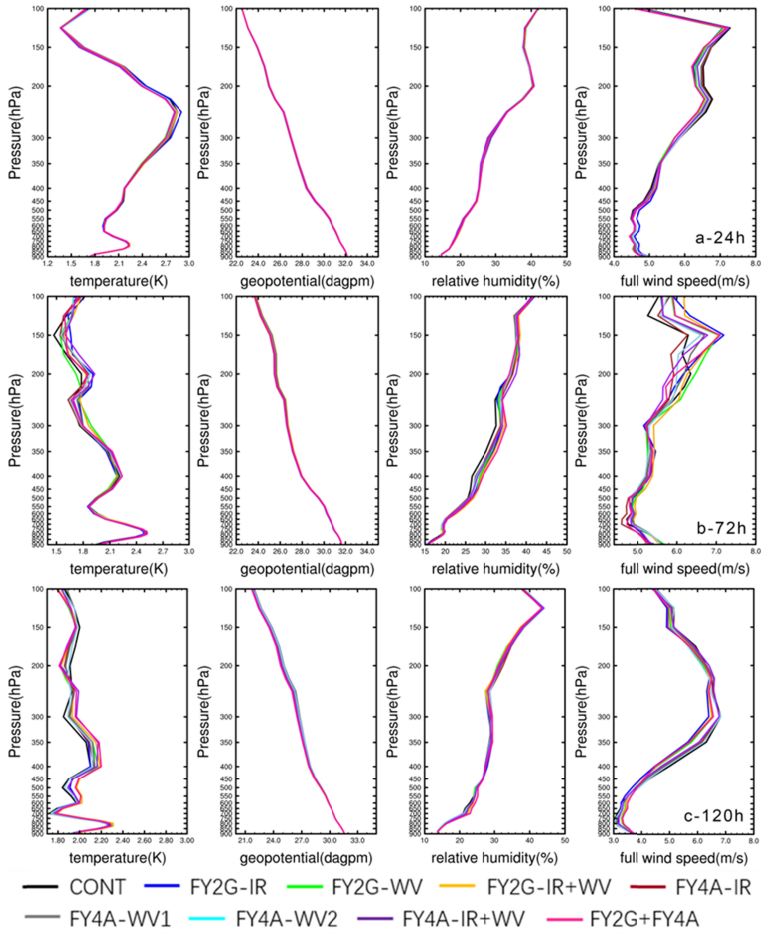

Figure 13. Vertical profiles of the 24-h (a), 72-h (b), and 120-h (c) forecast RMSEs versus the ECMWF ERA5 reanalysis of temperature (unit: K), geopotential height (unit: dagpm), relative humidity (unit: %) and the full wind speed (unit: m s−1) fields from the control experiment (CONT) (black), FY2G − IR (blue),FY2G − WV (green), FY2G − IR + WV (yellow), FY4A − IR (dark purple), FY4A− WV1 (gray), FY4A-WV2(light blue), FY4A_IR+WV(purple) and FY2G+FY4A(purple red).

6 Conclusion and Discussion

In order to evaluate the quality, assimilating and forecasting impacts of the AMVs data retrieved from the Chinese second generation geostationary meteorological satellite FY-4A in the typhoon forecasts within a limited domain by applying the WRFDA system with the 3D-VAR component, the AMVs from the first generation geostationary meteorological satellite FY-2G are used as an assessing reference in the overlapping observing region of the two. This study indicate that the retrieved AMVs from the infrared and water vapor channels of the two Fengyun satellites are mainly located at the middle and upper levels (100hPa to 700hPa) and only a few at the low level (700hPa to 950hPa), which are consistent with previous AMVs studies. For full

wind speeds, FY-4A AMVs show generally better data quality with smaller and stable RMSEs and biases than those of FY-2G.

Typhoon In-Fa is selected and eight cycling assimilation experiments and one control run are carried out to study the impacts of assimilation and forecasting by assimilating the two AMVs data on the typhoon forecasts, which are exhibited to be basically comparable for the forecasted typhoon tracks. Convincingly, assimilating the AMVs of both FY-2G and FY-4A can slightly reduce the track errors compared with CONT. However, there are no significant positive impacts for the typhoon intensity prediction and only neutral impacts are founded, which indicates that the typhoon intensity prediction is still a hard question for the NWP.

It is noticed that the experiments with the AMVs retrieved from water vapor channels are more likely to cause excessive rainfall amount in the typhoon precipitation prediction over land than those from infrared channels. Moreover, the physical variables field forecasts illustrate that assimilating the AMVs data from Fengyun geostationary satellites has neutral to positive impacts on the full wind speed more evidently than other physical variables fields vertically and the impacts extend from the upper level down to the lower level with time evolution since there are the largest number of the AMVs data at the upper level. The verification experiment of typhoon Haishen confirms the conclusions above by showing the similar assimilating and forecasting results.

As the new generation of Chinese geostationary satellite in meteorology, FY-4A has not only upgraded its instruments, but also provide data with better quality than its predecessor FY-2G. The results in the studies here are quite encouraging for the NWP application. Though the forecasting and assimilating impacts are basically neutral to slightly positive, the retrieved AMVs data are still worthy of being further investigated in order to be applied operationally. Lately, more FY-4 satellite series are about to be launched subsequently and more AMVs data can be retrieved from multiple channels and applied not only for the NWP, but also for various research purposes.

Acknowledgments

The authors appreciate the National Natural Science Funds of China to support this research through Grant No. 41875039 and also thank the National Key Scientific and Technological Infrastructure project “Earth System Science Numerical Simulator Facility” (EarthLab) for its support (Grant No.:2022-EL-PT-00052). The FY2G and FY4A AMVs data were obtained freely from (http://satellite.nsmc.org.cn/portalsite/Data/DataView.aspx/). The ECMWF analysis and the NCEP data can be downloaded from (https://cds.climate.copernicus.eu/cdsapp#!/dataset/reanalysis-era5-pressure-levels) and (https://rda.ucar.edu/datasets/ds083.3/), respectively. The precipitation observations can be obtained from (http://data.cma.cn/data/cdcindex/cid/f0fb4b55508804ca.html/).

References

Barker D M, Huang W, Guo Y R, et al. A three-dimensional variational (3DVAR) data assimilation system for use with MM5[J]. NCAR Tech Note, 2003, 68. https://doi.org/10.5065/D6CF9N1J

Barker D, Huang X Y, Liu Z, et al. The weather research and forecasting model's community variational/ensemble data assimilation system: WRFDA[J]. Bulletin of the American Meteorological Society, 2012, 93(6): 831-843.https://doi.org/10.1175/BAMS-D-11-00167.1

Bedka, K. M., Velden, C. S., Petersen, R. A., Feltz, W. F., & Mecikalski, J. R. (2009). Comparisons of satellite-derived atmospheric motion vectors, rawinsondes, and NOAA wind profiler observations. Journal of Applied Meteorology and Climatology, 48(8), 1542– 1561. https://doi.org/10.1175/2009JAMC1867.1

Dudhia, J. (1989). Numerical study of convection observed during the winter monsoon experiment using a mesoscale two-dimensional model. Journal of the Atmospheric Sciences, 46(20), 3077–3107. https://doi.org/10.1175/1520-0469(1989)046<3077:nsocod>2.0.co;2

Fairall, C. W., Bradley, E. F., Hare, J. E., Grachev, A. A., & Edson, J. B. (2003). Bulk parameterization of air-sea fluxes: Updates and verification for the COARE algorithm. Journal of Climate, 16(4), 571–591. https://doi.org/10.1175/1520-0442(2003)016<0571:BPOASF>2.0.CO;2

Hansen M C，Reed B．A comparison of the IGBP DIS Cover and University of Maryland 1 km global land cover products［J］．Int J Remote Sens，2000，21(6):1365-1373．21 https://doi.org/10.1080/014311600210218

Hong, S. Y., Noh, Y., & Dudhia, J. (2006). A new vertical diffusion package with an explicit treatment of entrainment processes. Monthly Weather Review, 134(9), 2318–2341. https://doi.org/10.1175/mwr3199.1

Huang, X.Y., Q. Xiao, D.M. Barker, X. Zhang, J. Michalakes, W. Huang, T. Henderson, J. Bray, Y. Chen, Z. Ma, J. Dudhia, Y. Guo, X. Zhang, D.J. Won, H.C. Lin, and Y.H. Kuo, 2009: Four-Dimensional Variational Data Assimilation for WRF: Formulation and Preliminary Results. Mon. Wea. Rev., 137, 299–314. https://doi.org/10.1175/2008MWR2577.1

Janjic, Zavisa I., 1994: The Step–Mountain Eta Coordinate Model: Further developments of the convection, viscous sublayer, and turbulence closure schemes. Mon. Wea. Rev., 122, 927–945. https://doi.org/10.1175/1520-0493(1994)122%3c0927:TSMECM%3e2.0.CO;2

Kain, J. S. (2004). The Kain-Fritsch convective parameterization: An update. Journal of Applied Meteorology, 43, 170–181. https://doi.org/10.1175/1520-0450(2004)043<0170:tkcpau>2.0.co;2

Liang, J., Chen, K., & Xian, Z. (2021). Assessment of FY - 2G Atmospheric Motion Vector Data and Assimilating Impacts on Typhoon Forecasts. Earth and Space Science, 8(6), e2020EA001628. https://doi.org/10.1029/2020EA001628

Li, Y., K. Y. Chen, and Z. P. Xian, 2021: Evaluation of All-Sky assimilation of FY-3C/MWHS-2 on Mei-Yu precipitation forecasts over the Yangtze-Huaihe River Basin. Adv. Atmos. Sci., https://doi.org/10.1007/s00376-021-0401-y.

Liu Rui, Zhai Guoqing, Wang Zhanggui, et al. Experimental study on the influence of FY-2C Cloud Track Wind Data Assimilation on typhoon forecast [J]. Chinese Journal of Atmospheric Sciences, 2012, 36(2): 350-360. Doi: CNKI:SUN:DQXK.0.2012-02-012(in Chinese).

Lin, Y., Farley, R., & Orville, H. (1983). Bulk parameterization of the snow field in a cloud model. Journal of Climate and Applied Meteorology,22, 1065–1092. https://doi.org/10.1175/1520-0450(1983)022<1065:BPOTSF>2.0.CO;2

Lu F，Zhang X H，Chen B Y，et al.，2017.FY-4 geostationary meteorological satellite imaging characteristics and its application prospects[J].J Mar Meteor，37（2）：1-12.doi：10.19513/j.cnki.issn2096-3599.2017.02.001.（in Chinese）.

Mecikalski, J. R., & Bedka, K. M. (2006). Forecasting convective initiation by monitoring the evolution of moving cumulus in daytime GOES imagery. Monthly Weather Review, 134(134), 49– 78. https://doi.org/10.1175/MWR3062.1

Mecikalski, J. R., Bedka, K. M., Paech, S. J., & Litten, L. A. (2008). A statistical evaluation of GOES cloud-top properties for nowcasting convective initiation. Monthly Weather Review, 136(12), 4899– 4914. https://doi.org/10.1175/2008MWR2352.1

Mlawer, E. J., Taubman, S. J., Brown, P. D., Iacono, M. J., & Clough, S. A. (1997). Radiative transfer for inhomogeneous atmospheres:RRTM, a validated correlated-k model for the longwave. Journal of Geophysical Research, 102(D14), 16663–16682. https://doi.org/10.1029/97JD00237

Niu, Guo–Yue, Zong–Liang Yang, Kenneth E. Mitchell, Fei Chen, Michael B. Ek, Michael Barlage, Anil Kumar, Kevin Manning, Dev Niyogi, Enrique Rosero, Mukul Tewari, Youlong Xia, 2011: The community Noah land surface model with multiparameterization options (Noah–MP): 1. Model description and evaluation with local–scale measurements. J. Geophys. Res., 116, D12109. https://doi.org/10.1029/2010JD015139

Peng Zhang, Qiang Guo, Boyang Chen, Xuan Feng. Comparative analysis of Chinese Fy-4 meteorological satellite and Japanese Himawari-8/9 satellite [J]. Progress in meteorological science and technology,2016,6(01):72-75(in Chinese).

Salonen K, Cotton J, Bormann N, et al. Characterizing AMV Height-Assignment Error by Comparing Best-Fit Pressure Statistics from the Met Office and ECMWF Data Assimilation Systems[J]. J.appl.meteor.climatol, 2014, 54(42):5647-5653. https://doi.org/10.1175/JAMC-D-14-0025.1

Tiedtke, M., 1989: A comprehensive mass flux scheme for cumulus parameterization in large–scale models. Mon. Wea. Rev., 117, 1779–1800.https://doi.org/10.1175/1520-0493(1989)117<1779:ACMFSF>2.0.CO;2

Velden C S, Bedka K M. Identifying the Uncertainty in Determining Satellite-Derived Atmospheric Motion Vector Height Attribution[J]. Journal of Applied Meteorology & Climatology, 2009, 48(3):450-463. https://doi.org/10.1175/2008JAMC1957.1

Xue, J. (2009). The scientific problems and prospects of meteorological satellite data assimilation. Acta Meteorologica Sinica, 67(6), 903– 911 (in Chinese). https://doi.org/10.3321/j.issn:0577-6619.2009.06.001

Yang Jun, et al. Meteorological satellites and their applications. Beijing: China Meteorological Press, 2012(in Chinese)

Figures Captions:

Figure 1. The observation area of geostationary satellites FY-2G and FY-4A (the red circle is for FY-2G; the yellow circle is for FY-4A; the green box is the studied area here; the solid line is for the northern hemisphere; the dotted line is for the southern hemisphere).

Figure 2. The vertical distributions of the RMSE (upper row) and the bias (lower row) of the full wind speed of the AMVs data retrieved from the infrared channels for the Northern Hemisphere referring to the ERA5 global reanalysis data. ((a) and (c) are for FY-2G, and (b) and (d) are for FY-4A. Red line represents the AMVs with QI larger than 80, blue line represents the AMVs with QI between 70 and 80, green line represents the AMVs with QI smaller than 70.

Figure 3. The RMSE time series of the AMVs data retrieved from the infrared channels at different height levels from August 1 2020 to October 31 2020. The red line represents the AMVs data with QI larger than 80; the blue line represents the AMVs data with QI between 70 and 80; and the green line represents the AMVs data with QI smaller than 70. (a), (c), (e) are for FY-2G and (b), (d), (f) are for FY-4A. The upper row are for 100 ~400hPa; the middle row are for 400 ~700hPa; and the lower row are for 700 ~950hPa.

Figure 4. The Probability density distribution of the first guess departures (O-B) of the AMVs data retrieved from the infrared channels of FY-2G and FY-4A after quality control processes at 12:00 UTC on July 22, 2020 (a for FY2G, b for FY4A, and c for the combined FY2G and FY4A).

Figure 5. The CMA best track of In-Fa from 0000 UTC on July 23, 2021 to 2100 UTC on July 27, 2021 (interval: 6h; TD: Tropical Depression TS: Tropical Storm; STS: Severe Tropical Storm; TY: Typhoon).

Figure 6. The evolution of track (a-c) referring to the CMA best track of Typhoon In-Fa from 0000 UTC on July 23 2021 to 0000 UTC on July 28 2021 (interval:6h; red: CMA best track; black: CONT; for a-c). For (a), yellow line represents experiment FY2G-IR+WV; green line represents experiment FY2G-WV; blue line represents experiment FY2G-IR. For (b), yellow line represents experiment FY4A-IR+WV; light blue line represents experiment FY4A-WV2; green line represents experiment FY4A-WV1; blue line represents experiment FY4A-IR. For (c), blue line represents experiment FY2G+FY4A.

Figure 7. The evolution of intensity (MSLP, unit: hPa) and track errors (b-c unit: km) referring to the CMA best track data of Typhoon In-Fa from 0000 UTC on July 23 2021 to 0000 UTC on July 28 2021, the time interval is 6h. (black line and bar: CONT; blue line and bar: FY2G-IR; green line and bar: FY2G-WV; orange line and bar: FY2G-IR+WV; brown line and bar: FY4A-IR; grey line and bar: FY4A-WV1; light blue line and bar: FY4A-WV2; purple line and bar: FY4A-IR+WV; pink line and bar: FY2G+FY4A; for a-c). For (a), red line represents the CMA best track.

Figure 8. The 24-h accumulated precipitation (unit: mm) over land from 0000 UTC on July 27, 2021 to 0000 UTC on July 28, 2021 from CMA observations of the hourly intensive automatic rainfall stations (a), CONT (b), FY2G−IR (c), FY2G-WV (d), FY2G-(IR+WV) (e), FY4A−IR (f),FY4A-WV1 (g),FY4A-WV2(h),FY4A-(IR+WV)(i) and FY2G+FY4A(j) experiments.

Figure 9. Vertical profiles of the 24-h (a), 72-h (b), and 120-h (c) forecast RMSEs referring to the ECMWF ERA5 reanalysis data of temperature (unit: K), geopotential height (unit: dagpm),

574 relative humidity (unit: %) and the full wind speed (unit: m s−1) fields started from 0000 UTC
575 on July 23 2021 from the control experiment (CONT) (black), FY2G − IR (blue),FY2G − WV
576 (green), FY2G − IR + WV (yellow), FY4A − IR (dark purple), FY4A− WV1 (gray), FY4A-
577 WV2(light blue), FY4A_IR+WV(purple) and FY2G+FY4A(purple red).

578 Figure 10. The CMA best track of Haishen from 0000 UTC on September 4, 2020 to 1200 UTC
579 on September 8, 2020 (interval: 6h; TD: Tropical Depression; TS: Tropical Storm; STS: Severe
580 Tropical Storm; TY: Typhoon STY: Severe Typhoon; SuperTY: Super Typhoon).

581 Figure 11. The evolution of track (a-c) referring to the CMA best track of Typhoon Haishen from
582 0000 UTC on September 4, 2020 to 1200 UTC on September 8, 2020 (interval:6h; red: CMA
583 best track; black: CONT; for a-c). For (a), yellow line represents experiment FY2G-IR+WV;
584 green line represents experiment FY2G-WV; blue line represents experiment FY2G-IR. For (b),
585 yellow line represents experiment FY4A-IR+WV; light blue line represents experiment FY4A-
586 WV2; green line represents experiment FY4A-WV1; blue line represents experiment FY4A-IR.
587 For (c), blue line represents experiment FY2G+FY4A.

588 Figure 12. The evolution of intensity (a MSLP, unit: hPa) and track errors (b-c unit: km)
589 referring to the CMA best track of Typhoon Haishen from 0000 UTC on September 4, 2020 to
590 1200 UTC on September 8, 2020 (black: CONT; blue: FY2G-IR; green: FY2G-WV; orange:
591 FY2G-IR+WV; brown: FY4A-IR; grey: FY4A-WV1; light blue: FY4A-WV2; purple: FY4A-
592 IR+WV; pink: FY2G+FY4A; for a-c). For (a), red line represents CMA best track.

593 Figure 13. Vertical profiles of the 24-h (a), 72-h (b), and 120-h (c) forecast RMSEs versus the
594 ECMWF ERA5 reanalysis of temperature (unit: K), geopotential height (unit: dagpm), relative
595 humidity (unit: %) and the full wind speed (unit: m s−1) fields from the control experiment
596 (CONT) (black), FY2G − IR (blue),FY2G − WV (green), FY2G − IR + WV (yellow), FY4A −
597 IR (dark purple), FY4A− WV1 (gray), FY4A-WV2(light blue), FY4A_IR+WV(purple) and
598 FY2G+FY4A(purple red).
599
600
601
602
603
604
605
606
607
608
609
610
611

612 Table 1: The channels used for retrieving the AMVs of geostationary satellite FY-2G and
613 FY-4A.

Satellite	IR Channel (μm)	WV Channel（μm）	Observing Area	Nadir
FY-2G	10.3-11.3	6.3-7.6	55°E-155°E 50°S-50°N	99.5°E
FY-4A	10.3-11.3	6.9-7.3	40°E-170°E 65°S-65°N	105°E
		5.8-6.7		

614

615

616

617

618

619

620

621

622

623

624 Table 2: The List of the Assimilating Experiment Settings

Experiments	ID	Settings
Control experiment	CONT	Without data assimilated
	FY2G-IR	FY-2G AMVs data from the infrared channel assimilated

cycling assimilation experiments	FY2G-WV	FY-2G AMVs data from the water vapor channel assimilated
	FY2G-IR+WV	FY-2G AMVs data from the combined channels assimilated
	FY4A-IR	FY-4A AMVs data from the infrared channel assimilated
	FY4A-WV1	FY-4A AMVs data from the lower water vapor channel assimilated
	FY4A-WV2	FY-4A AMVs data from the higher water vapor channel assimilated
	FY4A-IR+WV	FY-4A AMVs data from the combined channels assimilated
	FY2G+FY4A	FY-2G+FY-4A AMVs data from all the five retrieved channels assimilated

Table 3: The List of the Parameterization Schemes Used for All the Nine Experiments for Typhoon In-Fa.

parameterization schemes	settings
Microphysics scheme	Lin (Lin et al, 1983)
Cumulus convection scheme	Tiedtke (Tiedtke, M. et al., 1989)
radiation scheme	RRTMG /RRTMG (Mlawer et al., 1997)

Planetary boundary layer scheme	MYJ (Janjic et al., 1994)
Land-surface scheme	Noah (Niu et al., 2011)

632

633

634

635

636

637

638

639

640

641 Table 4: The List of the Parameterization Schemes Used for all the Nine Experiments for
642 Typhoon Haishen.

The Physical Parameterization Schemes		Configurations
Microphysics Scheme		Lin (Lin et al., 1983)
Planetary Boundary Layer Scheme		Yonsei University scheme (Hong et al., 2006)
Radiation Scheme	Long-wave	RRTM scheme (Mlawer et al., 1997)
	Short-wave	Dudhia scheme (Dudhia, 1989)
Cumulus Convection Scheme		Kain-Fritsch scheme (Kain, 2004)
Land-Surface Scheme		MM5 similarity (Fairall et.al., 2003)

643